Nanoscale

PAPER

View Article Online
View Journal | View Issue

Cite this: *Nanoscale*, 2020, **12**, 944

The synthesis of switch-off fluorescent water-stable copper nanocluster Hg^{2+} sensors *via* a simple one-pot approach by an *in situ* metal reduction strategy in the presence of a thiolated polymer ligand template†

Jesús Benavides, Isabel Quijada-Garrido and Olga García *

The fabrication of stable fluorescent copper nanoclusters (CuNCs) in aqueous media is still challenging, despite the low price and potential biomedical applications. Herein, we report a facile and efficient strategy for assembling CuNCs using multifunctional thiolated copolymers with pH and thermoresponsive features. The new nanohybrids are formed *via* a simple one-pot approach through the reduction of a copper salt with hydrazine in the presence of a multithiolated polymer, which provides a template during nanocluster assembly and further efficient protection against oxidation and aggregation. Furthermore, the thermo- and pH-responsive properties of the pristine copolymers endow the nanohybrids with these stimuli-responsive features. The thiol content and the macromolecular size of the polymer ligands exert strong influences on the final photophysical properties of these new hybrid luminescent nanoclusters. The existence of stable bright greenish-yellow emission in water over long periods of time, the high photostability under UV irradiation and the strong oxidation resistance toward hydrogen peroxide of the hybrid CuNCs suggest that they have great promise for nanomedicine, bioassay and nanosensor use. Furthermore, the polymeric CuNCs obtained have been successfully tested as optical switch-off sensors for the sensitive and highly selective detection of Hg^{2+} in the presence of other metal ions in liquid and solid states. Finally, we demonstrate the practical application of the new hybrid to Hg^{2+} detection in human urine.

Received 1st October 2019,
Accepted 2nd December 2019

DOI: 10.1039/c9nr08439h

rsc.li/nanoscale

1. Introduction

Metallic nanoclusters (NCs), composed through the association of a few tens to hundreds of metal atoms, with capping ligands decorating the surface of the metal core, are currently of the utmost interest, mainly due to their practical versatility.[1,2] Since the sizes of NCs are comparable to the Fermi wavelength (<2 nm in diameter), many of the physical and chemical properties of the metal are altered. These nanoparticles of quantum size constitute a new class of nanomaterial; they exhibit discrete electronic structures and similar properties to small molecules, such as having size-dependent HOMO–LUMO transitions and high luminescence. In addition, they can also display chiral and/or magnetic properties.[3,4] Because of these attractive characteristics, as well as their chemical stability, ultra-small hydrodynamic diameters and adaptable surface properties, metallic nanoclusters are promising fluorescent probes for biomedical imaging and detection, also showing extraordinary luminescence and low toxicity.[5–8]

As a result of these outstanding properties, in the last decade important advances in the development of fluorescent NCs, mainly involving Au and Ag, have been made.[9–11] On the other hand, non-precious metals such as copper (Cu) are very abundant, significantly cheaper and widely used in industry, also offering unique photoluminescence, optoelectronic and catalytic properties.[12–14] However, studies of CuNCs are still at the preliminary stage in relation to the progress achieved in relation to noble metals (Au and Ag), mostly due to difficulties controlling the synthesis at the sub-nanometer scale, the high tendency of CuNCs to aggregate, and the high susceptibility of CuNCs to oxidize upon exposure to air; therefore, the preparation of photoluminescent and stable CuNCs is a major challenge.[2]

Some recent literature articles have focused on achieving protected CuNCs; almost all of these refer to the use of mole-

Instituto de Ciencia y Tecnología de Polímeros (ICTP-CSIC), C/Juan de la Cierva, 3, E-28006-Madrid, Spain. E-mail: ogarcia@ictp.csic.es

†Electronic supplementary information (ESI) available. See DOI: 10.1039/c9nr08439h

cular ligands bearing functional groups that are able to conjugate with the metallic surface, such as different thiolated molecules, amino acids, or even small proteins.[15–22] Most of these authors have postulated that thiol groups are responsible for the reduction and functionalization of CuNCs. In all cases, brush-type functionalized CuNCs with emission centered in the red/blue region of the visible spectrum have been obtained, and their emissive properties are highly dependent on the pH of the medium.[14,22–24]

Intriguingly, these as-prepared CuNCs exhibit aggregation induced emission (AIE) behavior: molecules that are non-emissive in the solution state are induced to emit light upon the formation of aggregates.[2,14,15,21–24] Therefore, self-assembly driven by pH, solvent, temperature, or even mechanical strength can significantly revamp the luminescence behavior of nonluminescent or weakly luminescent NCs.[2,14,15,21–25] Moreover, unlike monodispersed individual CuNCs, an AIE-based strategy often requires the CuNCs to form large aggregates that are unstable in aqueous suspensions, which hampers their application when nanomaterials with good water solubility are demanded. Therefore, the development of a process to synthesize bright and highly fluorescent CuNCs, less dependent on the external conditions, that are soluble and stable in aqueous environments would create a wide range of possibilities for practical applications, mainly in the biomedical field.

Inspired by this challenge and based on our previous experience relating to the synthesis of fluorescent nanoparticles decorated with functional polymers (QDs,[26–29] UCNPs[30] and AgNPs[31]), in this work we propose to use polymers with multithiol groups that serve as ligands and templates for the synthesis, functionalization and stabilization of CuNCs. Therefore, new multithiolated polymers, soluble in water and stimuli-responsive (pH and temperature), have been designed and used to develop a new functionalization strategy that is simple, versatile and reproducible, allowing this type of photoluminescent nanohybrid to be obtained. The influences of different synthetic and methodological aspects and the influences of chemical structure and environmental factors on the final luminescent properties have been evaluated.

2. Experimental section

2.1 Materials

The monomer 2-(2-methoxyethoxy)ethyl methacrylate (MEO_2MA, Aldrich, 95%) was purified by passing it through a neutral column to remove the antioxidant inhibitor; the thiolated co-monomer, 2-(acetylthio)ethyl methacrylate (AcSEMA), with a protected thiol group was synthesized according to a protocol previously described by our group.[26] For the synthesis of the monomer, potassium thioacetate (Aldrich, 98%), triethylamine (Aldrich, ≥99%), 2-bromo-ethanol (Aldrich, 99%) and methacryloyl chloride (Aldrich, 99%) were used as received. For ATRP copolymerization, 1,1,4,7,10,10-hexamethyltriethylenetetramine (HMTETA, 99%, Aldrich), ethyl 2-bromoisobutyrate (EBr^iB, 99%, Aldrich), CuCl (99.99%, Aldrich), and the solvent benzonitrile (99.6%, Panreac) were used as received.

For synthesis of copper nanoclusters, the salt precursor of copper(II) sulfate pentahydrate ($CuSO_4{\cdot}5H_2O$, 98%, Aldrich), NaOH (Panreac, 85%) and hydrazine monohydrate ($N_2H_4{\cdot}H_2O$, Aldrich, 98%) were used as received. Phosphate buffered saline (PBS) solutions at different pH values were prepared using anhydrous sodium dihydrogen phosphate (Fluka, ≥99%), disodium hydrogen phosphate (Panreac, ≥98%), orthophosphoric acid (Panreac, 85%) and sodium chloride (Panreac, ≥99.5%) to keep the ionic strength constant.

For the stability studies, hydrogen peroxide (H_2O_2, Panreac, 33% w/v) and different metallic salts (lithium carbonate (Li_2CO_3, Panreac, ≥99.9%), sodium nitrate ($NaNO_3$, Aldrich, ≥99.9%), potassium carbonate (K_2CO_3, Panreac, ≥99.9%), sodium bromide (NaBr, Panreac, ≥99%), cadmium perchlorate hydrate ($Cd(ClO_4)_2{\cdot}H_2O$, Aldrich, ≥99.5%), lead(II) nitrate ($Pb(NO_3)_2$, Aldrich, ≥99%), nickel nitrate hexahydrate ($Ni(NO_3)_2{\cdot}6H_2O$, Fluka, ≥98.5%), zinc perchlorate hexahydrate ($Zn(ClO_4)_2{\cdot}6H_2O$, Aldrich, ≥99%), cobalt sulfate heptahydrate ($CoSO_4{\cdot}7H_2O$, Panreac, ≥99.9%), mercury(II) chloride ($HgCl_2$, Panreac, ≥99.9%), iron(II) chloride tetrahydrate ($FeCl_2{\cdot}4H_2O$, Aldrich, ≥99%) and iron(III) chloride hexahydrate ($FeCl_3{\cdot}6H_2O$, Aldrich, ≥99.9%)) were all used as received. The water used was Milli-Q water, obtained from a water purification facility (Millipore Milli-U10). Solvents were dried *via* standard methods or *via* elution through a Pure Solv Innovative Technology column drying system. Unless otherwise noted, reagents were commercially available and used without further purification.

2.2. Synthesis of p(MEO_2MA-*co*-AcSEMA) copolymers *via* atom transfer radical polymerization (ATRP)

ATRP copolymerization (Fig. 1A) was carried out in benzonitrile solution at 70 °C, using the monomer/initiator/ligand/catalyst (M/I/L/C) ratios and reaction times indicated in Table 1.[27] A typical procedure for the synthesis of these statistical copolymers is described for the sample **P2-C**: HMTETA (0.041 g, 0.18 mmol), MEO_2MA (4.750 g, 25.24 mmol), AcSEMA (0.250 g, 1.33 mmol), CuCl (0.017 g, 0.18 mmol) and benzonitrile (5 g) were added to a Schlenk flask, which was then immersed in an ice-water bath; after the solution was degassed *via* purging with nitrogen for 20 min, the initiator ethyl-2-bromoisobutyrate (EBr^iB; 0.034 g, 0.177 mmol) was introduced into the flask *via* a nitrogen degassed syringe. The Schlenk flask was immediately immersed in an oil bath at 70 °C. After 90 min, to stop the reaction, the mixture was cooled, opened to air and quenched with chloroform and then it was passed through a neutral alumina column to remove the catalyst. The solution was concentrated *via* rotary evaporation and then the polymer was precipitated *via* adding the solution to a large excess of *n*-hexane. The precipitated product was decanted and dried under high vacuum until a constant weight was reached. The total monomer conversion was measured gravimetrically.

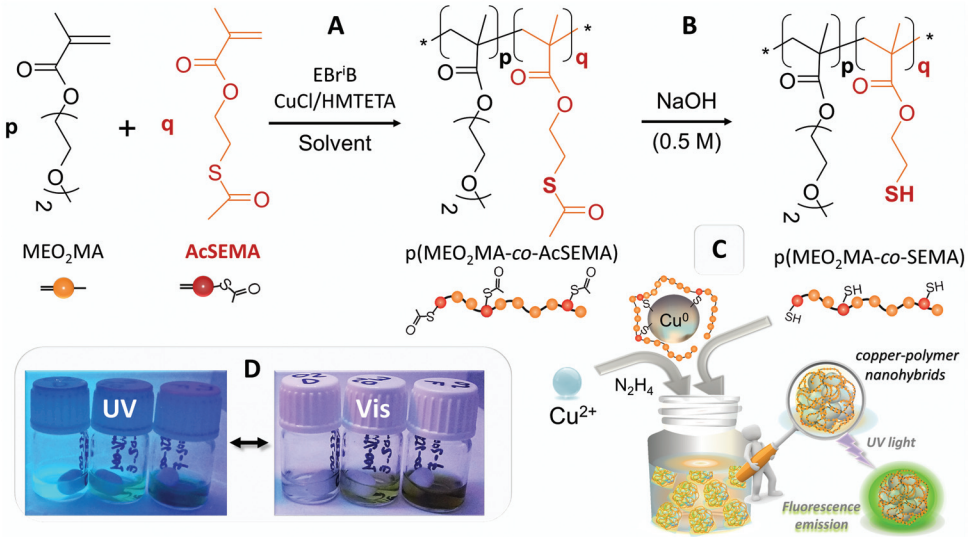

Fig. 1 (A) The copolymerization process for the synthesis of p(MEO$_2$MA-*co*-AcSEMA) copolymers *via* ATRP and (B) their subsequent hydrolysis in basic solution to produce p(MEO$_2$MA-*co*-SEMA) multithiolated functional polymers. (C) A schematic illustration of the one-pot synthesis process of fluorescent hybrid copper nanoclusters (CuNCs). (D) Photographs of hybrid CuNCs under both UV and visible light illumination are shown.

Table 1 The experimental synthetic conditions and characterization of p(MEO$_2$MA-*co*-AcSEMA) (P*n*-X) copolymers synthesized *via* ATRP in benzonitrile at 70 °C

Polymer	Time (min)	M/I/L/C	F_{AcSEMA} [a]	Conv. (%)	$M_{w\ SEC}$ [b] (g mol^{-1})	PDI[c]	T_{cp} [d] (°C)
P2-C	90	150/1/1/1	2.0	59	28 875	1.19	27.6
P6-A	45	65/1/1/1	5.9	78	11 692	1.17	20.3
P6-B	90	130/1/1/1	5.8	82	22 469	1.18	20.4
P6-C	135	195/1/1/1	6.0	70	36 667	1.24	20.0
P6-D	180	260/1/1/1	6.0	65	47 361	1.34	19.3
P8-B	135	195/1/1/1	8.5	76	20 946	1.29	16.9
P8-D	180	260/1/1/1	8.3	75	36 706	1.24	17.0
P13-B	90	143/1/1/1	13.5	80	22 570	1.12	12.9

[a] F_{AcSEMA}: Experimental molar fraction of AcSEMA in the copolymer (calculated *via* ^{1}H NMR). [b] M_w: Average molecular weight (determined *via* SEC). [c] PDI = M_w/M_n: polydispersity index. [d] T_{cp}: The cloud point temperature of the polymer aqueous solution (1 mg mL^{-1}), determined *via* UV/vis measurements. For comparison, the T_{cp} value for p(MEO$_2$MA) is 28.0 °C.[33,34]

Before the polymers could be used as templates and ligands for CuNC synthesis, thioacetate groups were converted into thiols (Fig. 1B). For this, basic solutions of all the obtained copolymers were prepared (4 mM in 0.5 M NaOH); the hydrolysis process was followed using ^{1}H NMR and FTIR-ATR analysis (Fig. S1†).

2.3. Synthesis of fluorescent hybrid copper nanoclusters

One-pot monodisperse highly fluorescent new copper nanoclusters (CuNCs) protected with multithiolated thermoresponsive polymer ligands, Cu@p(MEO$_2$MA-*co*-SEMA), denoted as Cu@P*n*-X hybrid nanoparticles from now on, were synthesized *via* the one-pot method presented in Fig. 1C. The letter P denotes the thiolated p(MEO$_2$MA-*co*-SEMA) copolymer contribution, *n* refers to the molar proportion of the SEMA thiolated comonomer in the polymer, and the letter X indicates the molecular weight of the hydrolyzed copolymer (Table 1). A typical procedure for the synthesis of sample **Cu@P6-B** (2/2 mM) (6 mol% SEMA and ~20 kDa) is as follows: in the first instance, the reaction was performed *via* adding an aliquot (40 μL) of $CuSO_4$ (50 mM in water) to 0.96 mL of hydrolyzed P6-B copolymer solution (2 mM in 0.5 M NaOH). The organic–inorganic solution was incubated for 2 h under magnetic stirring in an ice-water bath to ensure the dissolution of the thermoresponsive copolymer. After this time, 32 μL of hydrazine monohydrate was added as a reducing agent and the mixture quickly became yellowish colored, confirming CuNC formation. The cooled mixture was vigorously stirred for an additional 1–3 h. The reaction, monitored *via* UV/vis absorbance and fluorescence emission analysis, was stopped when intense yellow-green fluorescence emission was detected under UV-light (Fig. 1). The final copper nanohybrids, without further purification, were stored in a refrigerator at 4 °C until required. To optimize the synthetic procedure used for the CuNC hybrids, different metal-to-polymer (Cu/P) molar ratios were used (Table S1†).

2.4. Characterization and properties

^{1}H NMR spectra were recorded using a Bruker 400 MHz spectrometer in $CDCl_3$ at room temperature. Polymer molecular weights and molecular weight distributions were determined using a Waters gel permeation chromatograph equipped with a Waters 1515 isocratic high-performance liquid chromatography (SEC) pump and Waters 2414 refractive index (RI) detector. Samples were eluted at a flow rate of 1 mL min^{-1} in HPLC grade tetrahydrofuran (THF). Polystyrene standards were used for calibration. Infrared spectra were obtained using a Spectrum One FTIR spectrometer (Perkin-Elmer) fitted with an attenuated total reflectance (ATR) accessory under unforced conditions. The samples were placed in direct contact with the diamond crystal without additional preparation and dried with a stream of hot air. Measurements were collected at a resolution of 6 cm^{-1} with 4 scans per spectrum.

UV/vis absorption and fluorescence spectra were recorded using PerkinElmer Lambda-35 and PerkinElmer LS5OB spectrophotometers, respectively. The fluorescence quantum yield (QY) (excitation at 400 nm) values of dilute aqueous solutions of hybrid CuNCs (abs <0.1 at 400 nm) were evaluated relative to rhodamine 6G dye in ethanol solution (QY = 0.95)[32] employing a small volume microcuvette (50 μL) in the fluorimeter at 90°. To study the fluorescence emission as a function of pH and temperature, one temperature below (4 °C) and one temperature above (50 °C) the cloud point (21–31 °C) were selected to analyze concentrated hybrid CuNC water solutions adjusted to different pHs (pH = 4, 7 and 12) *via* adding HCl (1 M) to pristine basic CuNC solution. Samples at the selected pH values were left to equilibrate at 4 °C before recording fluorescence emission spectra; after that, samples were equilibrated at 50 °C and fluorescence emission spectra were recorded, and so on. The samples were temperature-adjusted using a Huber-polycat cc1 cryostat system or a Julabo-paratherm U5-electronic thermostated bath. In all cases, the fluorescence signals were recorded in front-facing mode *via* orienting the immersed samples at angles of 35° and 55° with respect to the excitation and emission beams when measurements were conducted at different temperatures. The recorded fluorescence spectra were averages of at least three independent measurements made until reproducible fluorescence intensities were obtained.

The thermoresponsive behaviors of the polymers and CuNC hybrid aqueous solutions were studied after determining the cloud point temperature (T_{cp}); this was done by measuring changes in the optical absorbance at 700 nm at a concentration of 1 mg mL^{-1} as a function of temperature using a Cary 3 BIO-Varian UV-vis spectrophotometer equipped with a Peltier temperature control device. The temperature was raised from 10 to 60 °C at a rate of 1 °C min^{-1}. These measurements were also done employing solutions with different pH values. The pH was determined with Crison pH-meter GLP21 apparatus.

Dynamic light scattering (DLS) measurements of the hybrid CuNCs were performed using a Malvern Zetasizer Nano Z spectrometer with a 10 mW HeNe laser at 633 nm. All measurements were performed at a scattering angle of 173°. All diluted sample solutions were measured at a concentration of 1 mg mL^{-1} in water at different pH and temperature values.

Scanning transmission electron microscopy (STEM) images were recorded with a field emission scanning electron microscopy (FE-SEM) Hitachi-SU8000 microscope operating at 30 kV in transmitted-electron imaging mode, equipped with a charge-coupled device (CCD) camera. Usually, for sample preparation, one drop of functionalized CuNC solution in water (~5–10 μL) was left to dry under vacuum over ultrathin carbon type-A film supported on a 400 mesh copper grid (3 mm in diameter) (from Ted Pella, Inc.). In order to determine the thermally induced aggregation of hybrid CuNCs *via* STEM, the preparation of the hybrid nanoclusters was carried out as follows: about 5–10 μL of 1 mg mL^{-1} CuNC aqueous solution was left to dry under vacuum or under a warm air flow on a carbon film supported on the same type of copper grid.

X-ray photoelectron spectroscopy (XPS) measurements were carried out on a SPECS system, working at a pressure of 10^{-7} Pa with a monochromatic Al Kα X-ray source (1486.7 eV) operating at 14.00 kV and 150 W. The charge built up on the sample during XPS measurements was counteracted *in situ* by means of an electron gun.

The photostability properties of the hybrid CuNCs were assessed *via* irradiation under UV-light using a photoreactor (UVP, CL100-UVcrosslinker model) equipped with five UVA irradiation lamps with light emission centered at 365 nm, generating 34.2 W m^{-2}, experimentally measured with a spectroradiometer (v2.2, LuzChem). For photostability studies of the as-prepared CuNCs, the fluorescence emission signal (λ_{exc} = 400 nm) was recorded as a function of the UV-light irradiation time.

The resistance to oxidation was studied *via* incubating the samples (minimum of 1 h) in solutions of increasing hydrogen peroxide (H_2O_2) concentration and determining the effects on the fluorescence emission signal.

Experiments to explore the use of these hybrids as sensors to detect heavy metal ions were done *via* incubating samples (minimum of 1 h) in basic solutions of different metallic salts (at a concentration of 100 μM), and also incubating the hybrid CuNCs with solutions of increasing mercury(II) chloride ($HgCl_2$) salt concentration, and studying the evolution of the fluorescence emission signal.

In all stability experiments, emission spectra (λ_{exc} = 400 nm) were recorded employing a small volume microcuvette (50 μL) in the fluorimeter at 90° until a stable emission response was obtained (minimum of 5 measurements per experiment).

For solid-state assays, 5 μL of CuNC solution (2 mM) was dropped over a microscope slide and left to dry under vacuum. Then a drop (5 μL) of the analyte aqueous sample was deposited over the dry solid-state sensor and visualized under a UV lamp to detect emission changes.

Feasibility studies investigating the hybrid CuNCs as switch-off sensors for Hg^{2+} detection in real samples were directly performed in human urine, without any prior purifi-

cation. Fresh human urine samples were collected from La Paz University Hospital. The hybrid CuNCs were incubated at a constant concentration (0.8 mM) in the presence of increasing concentrations of mercury in urine (for the course of 30 min). In these practical experiments, the fluorescence emission recordings were optimized at λ_{exc} = 440 nm in order to avoid self-fluorescence emission from the pristine urine. A small volume microcuvette (50 μL) was also employed in the fluorimeter at 90° until a stable emission response was achieved (minimum of 3 measurements per experiment).

3. Results and discussion

The main goal of this study was to carry out the synthesis of highly fluorescent copper nanoclusters (CuNCs) *via* "*in situ*" functionalization with a thin thermoresponsive polymeric coating using a facile and low cost approach to overcome the drawbacks of existing methods (instability over time, limitations relating to the high dependence of the emissive properties on pH, incompatibility between the solubility of the aggregates and the AIE behavior, *etc.*).

According to our previous research involving luminescent NPs,[26–31] the polymeric shell may act as a protective coating to stabilize the CuNCs, preventing their aggregation and oxidation, keeping the size of the new nanohybrids on the nanometric scale, preserving the photophysical properties and offering, in addition, new properties with regards to water solubility, biocompatibility and even stimuli-responsivity.

Thus, we synthesized a family of copolymers based on an acetyl-protected thiol methacrylic monomer (AcSEMA)[26] and 2-(2-methoxyethoxy)ethyl methacrylate (MEO_2MA). The ATRP procedure used to obtain this series of well-defined hidden-thiol functionalized thermoresponsive polymers, p(MEO_2MA-*co*-AcSEMA), is outlined in Fig. 1A.

In Table 1, the experimental synthetic conditions, compositions, molecular weights and polydispersities of the selected copolymers are collected. The chemical structures and molar fraction compositions of the obtained copolymers were analyzed *via* ^{1}H NMR as well as FTIR-ATR (Fig. S1 in the ESI†).[35] The THF SEC results using polystyrene standards indicated that the polymerization processes were well controlled (Table 1); only small deviations between the feed molar fractions of AcSEMA and the experimentally derived values (F_{AcSEMA}) were detected, indicating slight differences in the reactivity of the monomer.

The molecular weight distributions are narrow and, therefore, polydispersity indices lower than 1.34 were observed in all cases. The polydispersity indices slightly increase with an increase in the molecular weight (Table 1). The resulting p(MEO_2MA-*co*-AcSEMA) copolymers show thermoresponsive properties comparable to poly(*N*-isopropylacrylamide), the most studied thermoresponsive polymer.[36,37]

The cloud point temperature (T_{cp}) values, determined *via* absorbance measurements, are also collected in Table 1. As can be observed, the introduction of AcSEMA into the copolymer increases the hydrophobic balance, giving rise to a decrease in the T_{cp} value as the AcSEMA content increases in the copolymer. Furthermore, after the hydrolysis of AcSEMA and due to the acidity of the thiol group, the thermoresponsive properties become dependent on the pH; at low pH, the thiol is protonated and T_{cp} is close to that of the p(MEO_2MA) homopolymer, whereas in a basic medium, the thiolate anion generates a dramatic increase in the cloud point temperature.[26,27] This behavior is illustrated in Fig. S2 in the ESI† for a hydrolyzed P6-B sample.

The synthesis and functionalization of the CuNCs with the thiolated polymers was carried out in water under mild reduction conditions. The procedure was simple, involving incubating the starting precursors (copper salt and hydrolyzed thiolated polymer) in basic water under continuous stirring at low temperature to ensure the complete dissolution of the polymer, before finally adding hydrazine as a reducing agent (see further details in the Experimental section).

The multithiol functionalization of the copolymers allowed for the collection and stabilization of highly luminescent water-soluble hybrid CuNCs (Fig. 2). The primary and unequivocal experimental evidence showing the formation of CuNCs is found in the rapid increase of the fluorescence emission band as the incubation time increases, as shown in the example in Fig. 2 of the sample Cu@P6-B. It can be highlighted that the absence of the polymer and/or reducing agent did not give rise to the formation of fluorescent CuNCs.

Different techniques were applied for the characterization of the obtained polymeric nanoclusters (FTIR-ATR, STEM, DLS, XPS, *etc.*), and these results are collected in Table 2 and Fig. S3 in the ESI.† The FTIR-ATR spectra of the hybrid CuNCs display no significant differences compared to those of the hydrolyzed polymers used for the functionalization (Fig. S3A†). This shows that the chemical structures of the polymers did not change after coating on the CuNCs.

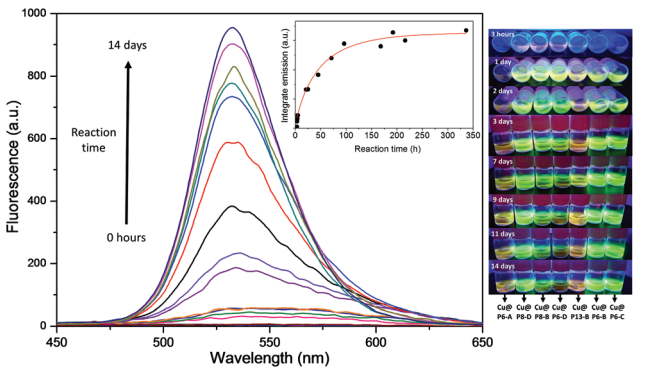

Fig. 2 The increase in the fluorescence emission band (λ_{exc} = 400 nm) with reaction time in the formation of CuNCs (sample: Cu@P6-B (2/2 mM)). The inset graph shows the evolution of the integrated emission signal with reaction time. On the right side, photographs of some hybrid CuNCs under UV-lamp illumination at different reaction times are shown; hybrids are synthesized using different polymers, as indicated in the text below the photographs.

Table 2 The photophysical and thermoresponsive properties of hybrid CuNCs synthesized and functionalized with thiolated p(MEO_2MA-*co*-SEMA) copolymers, P*n*-X, starting from equimolar proportions (2 mM) of the precursors

Hybrid[a]	$\lambda_{em\ max}$ [b] (nm)	%QY[c]	Time[d] (days)	T_{cp} [e] (°C) pH 4	Size[f] (nm) 10 °C	Size[f] (nm) 50 °C
Cu@P2-C	536.8	0.7	2	24.1	4 ± 2	2521 ± 489
Cu@P6-A	540.6	1.6	11	29.0	4 ± 1	1866 ± 476
Cu@P6-B	533.5	11.9	7	25.0	5 ± 1	1405 ± 326
Cu@P6-C	537.7	6.3	3	24.1	8 ± 2	1043 ± 280
Cu@P6-D	535.5	7.7	1	27.1	9 ± 2	38 ± 10
Cu@P8-B	536.9	9.0	1	25.0	6 ± 1	1956 ± 788
Cu@P8-D	532.6	2.8	1	26.1	7 ± 2	57 ± 12
Cu@P13-B	536.1	4.4	4	29.1	7 ± 2	508 ± 190

[a] Nanohybrids are obtained at a Cu/polymer ratio of 2/2 mM in all cases. [b] Maximum wavelength emission values are obtained in basic water (nm). [c] Fluorescence quantum yield (%QY) (excitation at 400 nm) values for the nanohybrids are obtained in dilute aqueous basic solutions relative to rhodamine 6G dye in ethanol solution (QY = 0.95).[32] [d] Time to reach the maximum QY. [e] T_{cp} is the cloud point temperature estimated in acidic water (pH 4) *via* UV/vis measurements. [f] Hydrodynamic size values by number are calculated from DLS measurements in acidic water (pH 4) at low (10 °C) and high (50 °C) temperatures, respectively.

We further used STEM to characterize the morphologies and sizes of these new CuNCs (Fig. S3B†). STEM showed that the hybrid CuNCs were always spherical in shape and uniformly dispersed with very small size, corroborating the DLS results that estimated sizes between 4 and 9 nm (Table 2). Meanwhile, we did not observe any visible large size metal nanoparticles or aggregation, agreeing well with our observations from DLS characterization.

Likewise, XPS analysis was carried out to determine the oxidation state of copper in the hybrid CuNC samples. Fig. S3Ci† displays the high-resolution spectrum of the Cu@P6-B hybrid, where the two peaks at 932.4 eV and 952.4 eV can be assigned to Cu(0) Cu $2p_{3/2}$ and Cu $2p_{1/2}$ electrons, respectively. The peaks are weak due to the polymer coating, which could have a thickness comparable to or even higher than the XPS analysis probe depth (~2–3 nm). Moreover, no characteristic satellite peak at around 942 eV can be seen, implying the absence of Cu(II) in the nanohybrids. However, from the XPS spectrum in Fig. S3Ci,† the presence of Cu(I) in the hybrid samples cannot be completely ruled out, since the binding energy due to Cu(0) $2p_{3/2}$ (932.4 eV) occurs ~0.1 eV apart from the Cu(I) peak. To clarify this fact, in Fig. S3Cii,† the Cu LMM Auger spectrum is presented; a main peak at 919.6 eV appears, which can be assigned to Cu(0) rather than to Cu(I).[38,39]

In order to obtain CuNCs with the brightest luminescence, the influence of different experimental conditions on the formation of these nanohybrids was evaluated (solvent, nature and amounts of reagents, type of reducing agent, times for the incubation of reactants and reactions, purification and storage methods, *etc.*). The results allowed the synthesis of these nanohybrids to be optimized and a direct relationship between the synthetic procedure, the CuNC structure and the final photophysical properties was established (Table S1 and Fig. S3–S6 in the ESI†).

The molar ratio of $CuSO_4$ to thiolated polymer was first optimized in the range from 0.5 to 5 mM for $CuSO_4$ and from 0.5 mM to 2 mM for the different polymers. From Fig. S4,† it is noted that the hybrid CuNCs with the brightest luminescence are obtained at a Cu/P*n*-X ratio of 2/2 mM, regardless of the copolymer used for capping. The great differences in the luminescence intensities clearly suggest that the ratio of initial precursors exerts a strong influence on the luminescence performance of the CuNCs. As a result, CuNCs with the brightest luminescence at the optimal reactant ratio (2/2 mM) were used for the following experiments relating to further characterization and applications; the data are shown in Table 2.

The formation of luminescent CuNCs has been observed for all copolymers tested for the synthesis of CuNCs, independent of the thiol content of the polymer or its molecular weight. This fact indicates the effectiveness of the thiol functionality for the capping and stabilization of CuNCs. Although the use of the P2-C copolymer with the lowest thiol content (2 mol%) results in suitable polymeric coverage and the formation of CuNCs, it also leads to hybrids that are less fluorescent and less stable over time, since in 3–4 weeks the CuNCs oxidize and form precipitates. Likewise, an excess of thiol groups produces similar behavior over time, as can be observed in Fig. S5† for the Cu@P13-B nanohybrids. As shown in Fig. 3 and Table 2, all the CuNC hybrids synthesized exhibit a faint absorption maximum at around 360 nm and remarkable fluorescence emission centered between 530 and 540 nm, depending on the copolymeric ligand employed, showing intense yellow-green emission under a UV lamp (insets of Fig. 2 and 3). Using this simple one-pot approach, light-yellow dispersions of the crude samples are obtained that are totally soluble, luminescent and stable in water for more than six months, even in the presence of air and/or without any protection from ambient light, as shown in Fig. S6.†

The effects of the monodentate multifunctional molecules on the CuNC surfaces and photophysical properties have been studied in detail by other authors. Thus, recently, two overviews of the topic have been published.[40,41] Different biomolecules have been tested as stabilizing ligands for red-emitting CuNCs on the basis of complexation and redox reactions

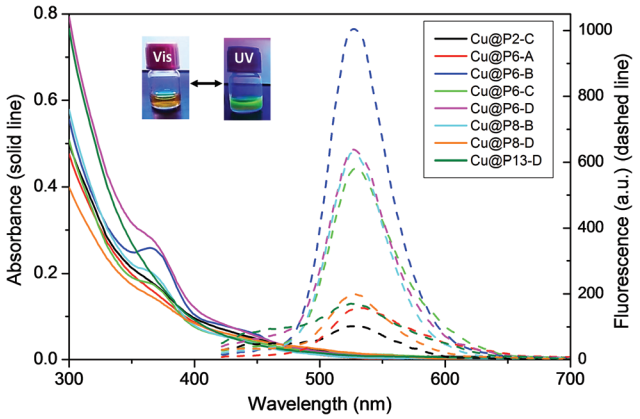

Fig. 3 The absorbance (solid lines) and emission fluorescence (λ_{exc} = 400 nm) (dashed lines) bands from dilute basic solutions of hybrid CuNCs (Cu@P*n*-X) synthesized with 2 mM solutions of p(MEO_2MA-*co*-SEMA) multithiolated copolymers, as specified in the legend. Inset: Photographs of Cu@P8-B (1.5/2 mM) hybrids under vis- and UV-light.

between copper(II) and different biomolecules, such as D-penillamine,[14,20,42] glutathione,[2,35] albumin,[18,43] and cysteine.[44,45] In addition to small ligands, macromolecules have been assayed, giving rise to green-emitting CuNCs with polyvinylpyrrolidone,[46] red-emitting CuNCs with β-galactosidase,[21] blue-emitting CuNCs with lysozyme,[47] and blue and yellow-emitting CuNCs stabilized with trypsin.[24] These results show how the photophysical properties of CuNCs may derive from both the metal core (quantum size effects) and from metal surface effects (interactions between the metal core and the surface ligands).[12,41,48]

In our case, the ligand capping molecule is a macromolecule with several hanging thiol groups that, in fact, acts as a multidentate thiolated ligand. We obtained, in all cases, hybrid CuNCs with intense yellow-green emission (around 535 nm) and high fluorescence QYs, in the region of those obtained by other authors.[42–47]

As shown in Table 2, no significant changes are observed in the emission band maxima of the nanohybrids with variations in the percentage of thiol present in the polymer or the molecular weight, although these parameters are critical for the obtained QY. The highest fluorescence QY values were obtained for polymers with intermediate thiol content values (6 or 8 mol%) and molecular weights of around 20 kg mol^{-1} (Table 2 and Fig. S6†). We also observed that increases in the thiol content and/or molecular weight of the polymer favor obtaining the best emission properties in a shorter time. To illustrate this behavior, in Table 2 it can be seen that for the Cu@P6-X nanohybrids, the time taken to reach the maximum QY decreases with an increase in the molecular weight, although the highest QY was reached for the Cu@P6-B (a polymer with $M_w \approx 22$ kg mol^{-1}). Comparing Cu@P6-B with Cu@P8-B (polymers with similar M_w values and different thiol content values), the maximum QY is reached in a shorter time for Cu@P8-B, however the absolute QY reached is higher in the case of Cu@P6-B (see Table 2 and Fig. S6†).

In all cases, the polymeric coverage is thin, maintaining a hybrid nanometric hydrodynamic size of between 4 and 9 nm (Table 2). For similar thiol content values, a slight increase in the nanohybrid size is detected with an increase in the M_w value of the copolymer employed.

Furthermore, the thermo- and pH-responsive properties of the pristine copolymers endow the nanohybrids with stimuli-responsive behaviors. In Fig. 4A, the absorbance values for hybrid CuNC aqueous solutions at pH 4 as a function of temperature show the existence of a cloud point temperature. The turbidity increase is a consequence of the formation of large aggregates above the critical temperature, as occurred for the hydrolyzed pristine copolymers (Fig. S2†).

Cloud point temperatures at pH 4, collected in Table 2, indicate a slight dependence on the chemical composition of the copolymer, being higher for CuNC hybrids with higher thiol content values; this can be attributed to an increase in the hydrophilicity. Compared with the thermal responses of the starting polymers, in general, the T_{cp} values of the hybrids are shifted by 5–10 °C to higher temperatures with respect to the T_{cp} values of the copolymers; this can obviously be attributed to the attachment of the thiol groups to the surface of the metal core. In fact, all the T_{cp} values of the hybrids are raised close to the homopolymer values (*ca.* 28 °C).[33,34] As occurs with the hydrolyzed copolymers (Fig. S2†), the thermo-responsive properties are enhanced in an acidic medium. The ionization of the thiol group, converting it into sodium thiolate, with increasing pH produces a progressive and strong increase in the hydrophilic balance that, at basic pH, gives rise to the disappearance of the cloud point. This fact is summarized in Fig. 4B for the sample Cu@P8-B. This behavior is fully reversible, so that after decreasing the pH below 7, the, cloud point is recovered.

The thermo-responsiveness of the hybrid CuNCs was also investigated at the nanoscale. Thus, Fig. 5 displays hydrodynamic size data determined *via* DLS, *Z*-potential values and STEM images of CuNC nanohybrids as a function of temperature (below and above T_{cp}) at pH 4. Fig. S7† shows the change in the CuNC hydrodynamic size with temperature (10 and 50 °C) and pH, as well as the *Z*-potential values obtained at basic pH values.

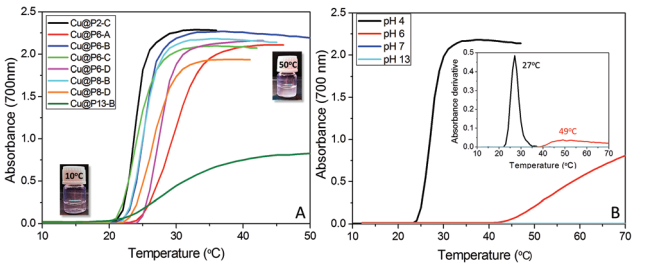

Fig. 4 Cloud points obtained from the absorbance at 700 nm of (A) solutions of Cu@P*n*-X nanohybrids at pH 4 diluted with water (1 mg mL^{-1}) and (B) dilute solutions of Cu@P8-B nanohybrids as a function of pH.

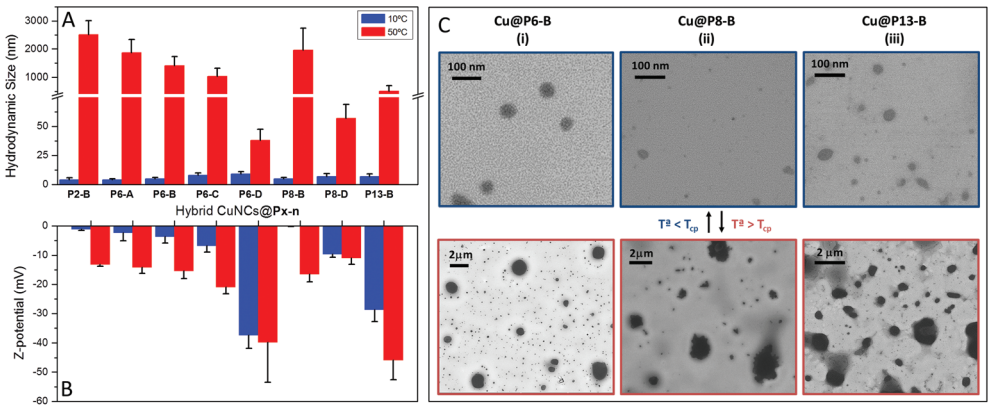

Fig. 5 (A) Hydrodynamic size and (B) *Z*-potential data from the Cu@P*n*-X nanohybrids obtained at a Cu/polymer proportion of 2/2 mM with the thiolated copolymers (P*n*-X), obtained *via* DLS measurements in acidic (pH 4) dilute solutions (1 mg mL^{-1}) below (10 °C: blue bars) and above (50 °C: red bars) T_{cp}. (C) STEM images below and above T_{cp} of the Cu@P6-B (i), Cu@P8-B (ii), and Cu@P13-B (iii) nanohybrids. (Note that all STEM samples were prepared from the same acid water solution, thus differences can only be attributed to temperature effects).

At low pH, the nanohybrids undergo a drastic decrease in solubility above a critical temperature, so that Cu@P*n*-X samples that exhibited diameters between 4 and 9 nm at 10 °C give rise to large aggregates at 50 °C with diameters of up to 1–2 μm, as can also be seen in the STEM images shown in Fig. 5C. A similar temperature-dependence is noticed for the hydrodynamic diameters at pH 6 (Fig. S7A†), while at pH 7 and pH 13 (Fig. S7B and S7C†), the hydrodynamic size barely varies with temperature. Once more, it should be noted that the solubility of the copolymer coating is enhanced at high pH due to the ionization of the thiol groups. An increase in the number of thiolate groups at high pH values prevents polymer collapse, except for the Cu@P2-C nanohybrids, as this hybrid with the lowest number of thiol groups exhibits the formation of large aggregates at 50 °C, even at pH 13 (Fig. S7C†). Following the hybrid size as a function of temperature *via* DLS, the collapse temperature can also be determined, and this is in good agreement with the cloud point measurements (Fig. S8†). This behavior can be directly related to the number of free thiol groups presents in the final hybrid, as indicated by the *Z*-potential values included in Fig. 5B. The *Z*-potential values at pH 4 and low temperature (Fig. 5B) are low, close to zero; since at this pH the polymer should be neutral, the low negative *Z*-potential values should be attributed to residual thiolate anions. However, at 50 °C polymeric collapse occurs, with the nanohybrids forming very large aggregates with a consequent increase in the *Z*-potential value above T_{cp} due to an increase in the charge density; however, for the higher molecular weight copolymers (P*n*-D), this collapse occurs but the change in size is not as drastic.

On the other hand, at basic pH, increases in the number of thiolate anions and the absorption of OH– result in an increase in *Z*-potential values at low temperature, providing good colloidal stability (Fig. S7D†). Since at high pH values the polymer coverage does not collapse, the *Z*-potential does not vary upon increasing the temperature to 50 °C.

Likewise, it was analyzed whether the pH- and thermo-responsive behaviors of the polymer coating also exerted some effects on the photoluminescence properties of the hybrid CuNCs. With this aim, fluorescence emission was tested at two temperatures, 4 and 50 °C, under basic, neutral and acidic pH conditions (Fig. 6A–C). At basic pH (pH 12), the polymer coating does not show any temperature response (Fig. 4B), since the sodium thiolate groups strongly increase the hydrophilic balance. The results shown in Fig. 6A indicate that at basic pH, the fluorescence emission is enhanced at low temperature. This behavior has been reported for CuNCs decorated with peptides,[49] AuNCs[50,51] and other types of luminescent NPs, such as silica.[52]

The decrease in fluorescence intensity at high temperature can be attributed to the thermal activation of several non-radiative channels. Comparing the integrated emission at 4 °C under acidic, neutral and basic pH conditions (Fig. 6D), we concluded that the highest emission occurs at alkaline pH values; since at this low temperature, the polymers are soluble at all three pH values (Fig. 4B), the increase in fluorescence at

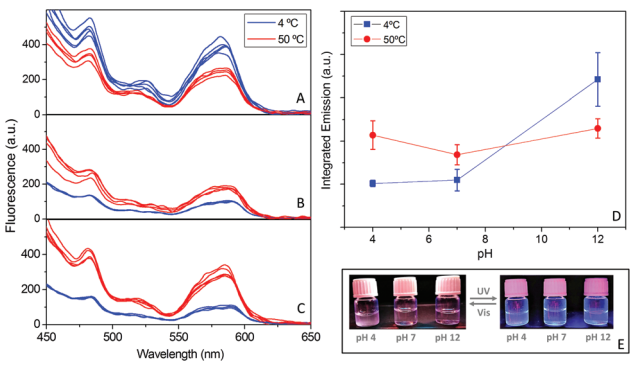

Fig. 6 Fluorescence spectra (λ_{exc} = 400 nm) of Cu@P6-B dissolved in water at (A) pH 12, (B) pH 7 and (C) pH 4, recorded in front-facing mode after heating the sample above (50 °C) and cooling below (4 °C) T_{cp} for consecutive cycles. (D) The evolution of the integrated fluorescence emission of Cu@P6-B in aqueous solution as a function of pH and temperature and (E) photographs of the dilute water solutions of Cu@P8-B at different pH values and room temperature.

high pH could be a consequence of the better passivation of the surface due the enhancement of the solubility of the hybrid in the medium. Contrary to what happens at pH 13, at neutral and acidic pH values the fluorescence emission increases with an increase in temperature, when the collapse of the hybrids occurs. This behavior is more pronounced at the lowest pH (Fig. 6C), where the integrated emission signal increases to more than twice its lower-temperature value. Thus, the collapse and subsequent aggregation, as observed *via* DLS and STEM analysis (Fig. 5A and C), lead to an amazing increase in the emission (1.5–2.1 times higher) (Fig. 6).

This significant improvement in fluorescence emission at acidic pH can be attributed to the energy transfer that occurs between the hybrid CuNCs due to the reduction of distance during the formation of aggregates as a result of collapse. The reduction in the spacing between the emitting cores hampers and even reverses the natural decrease in the fluorescence intensity that arises from heating.[50]

The same fluorescence emission responses to the temperature and pH of the medium were observed for all synthesized hybrids and are in full agreement with our previous research relating to the functionalization of other types of fluorescent NPs with these kinds of multithiolated polymers.[27,53]

For practical applications it is important to study the photo-/chemical stabilities of the new hybrid CuNCs to assess the degree of protection provided to the CuNCs by the polymeric coverage. Therefore, both the photostability and oxidation resistance properties of the hybrid CuNCs were tested against UV irradiation and different concentrations of hydrogen peroxide (H_2O_2, from 1 μM to 8 mM), respectively (Fig. S9†).

Firstly, the polymeric CuNCs were incubated with H_2O_2 solutions, and no significant variations in the fluorescence emission were observed, even when using high concentrations of H_2O_2, regardless of the thiol content of the copolymer used for the CuNC functionalization (see Fig. S9A†). This fact demonstrates the high resistance to oxidation of the as-synthesized polymeric CuNCs in accordance with those reported by other authors.[39,46]

Likewise, the hybrid CuNCs also exhibit high photostability *versus* UV-irradiation, as shown in Fig. S9B,† where it can be observed that the CuNCs need to be irradiated for at least 18 min with UV light (λ = 365 nm at a power intensity of 34.2 W m^{-2}) to achieve a 40% decrease in the fluorescence emission. According to our own experience, the new hybrid CuNCs show a clear improvement in photostability compared to polymeric silver nanoclusters (AgNCs),[31] which completely lose their emission under UV irradiation (at 365 nm) after 200–600 s depending on the polymeric coverage, even when using a lower power intensity (29 W m^{-2}). In this case, the decrease in fluorescence with irradiation time was attributed to the formation of large non-fluorescent silver nanoparticles from the aggregation of silver nanoclusters. But in this case, the irradiation light over the hybrid CuNCs only affects the emission intensity; no wavelength shifts or new emission bands are detected.

Additionally, as a proof-of-concept demonstration of their practical application, the as-prepared CuNCs have been investigated as visible "turn-off" sensors for different metal ions. The results, as reflected in Fig. 7A and Fig. S10,† showed that these new nanohybrids exhibit improvements in the selective detection of Hg^{2+} compared to other metal ions tested under the same experimental conditions (Li^+, Na^+, K^+, Br^-, Cd^{2+}, Pb^{2+}, Ni^{2+}, Zn^{2+}, Co^{2+}, Fe^{2+}, and Fe^{3+}). In fact, fluorescence emission decay of nearly 50% is detected in the presence of Hg^{2+}, whereas other metal ions induce only a slight (less than 10% for Co^{2+}) or negligible effect. In order to check the sensitivity of the hybrid nanoclusters, Stern–Volmer experiments were carried out in the presence of different concentrations of Hg^{2+}, as displayed in Fig. 7B. As shown in the example in the inset of Fig. 7B, the fluorescence emission of the hybrid CuNCs decreased significantly following their incubation with increasing concentrations of Hg^{2+}, showing high sensitivity and a linear response in the range of 1 nM to 100 μM of the quencher metal, regardless of the copolymer composition employed in the construction of the hybrid CuNCs. This be-

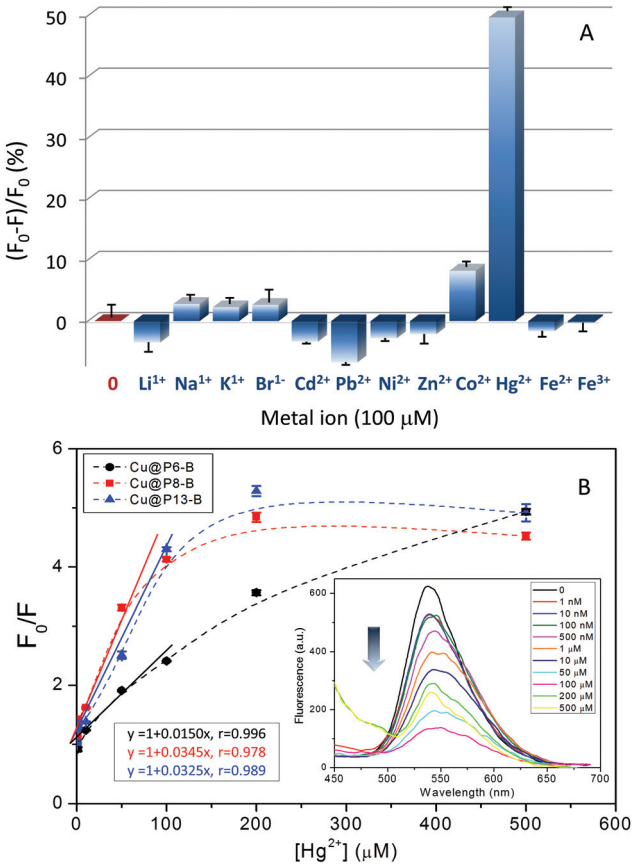

Fig. 7 (A) The selectivity of the Cu@P6-B hybrids towards different metal ions, measured *via* the changes in the emission properties in the presence of 100 μM concentrations of each metal ion. (B) A Stern–Volmer representation of the Cu@P*n*-B hybrids quenched by Hg^{2+}. Inset: The evolution of the fluorescence emission spectra of Cu@P8-B nanohybrids in the presence of increasing concentrations of Hg^{2+} (between 1 nM and 500 μM) (λ_{exc} = 400 nm) [the dashed lines represent the evolution of the obtained data and the solid lines correspond to the linear fit of the obtained data in the 0–100 μM range].

havior is similar to the results found by other authors using other types of functionalized CuNCs.[24,39,46]

To date, different Hg^{2+}-induced fluorescence quenching mechanisms have been proposed. Morishita *et al.*[54] proposed that the force driving Hg^{2+} to interact with AgNCs arises from redox reactions. Nevertheless, in the present case, other fluorescence quenching mechanisms should not be discarded, since our polymer coated CuNC hybrids exhibit high resistance to oxidation, as shown by the stable fluorescence emission in the presence of high concentrations of H_2O_2 (Fig. S9A†).

As previously reported,[24] the fluorescence quenching of the CuNCs could be ascribed to the aggregation of CuNCs induced by Hg^{2+}, thus facilitating efficient energy transfer. In addition, the fact that quenching by Hg^{2+} did not significantly affect either the fluorescence emission spectra (inset of Fig. 7B and Fig. S10†) or the absorption spectra of the CuNCs further indicates that the quenching mechanism involves energy transfer between the CuNCs and Hg^{2+}.

Indeed, after the incubation of the hybrid CuNCs with increasing concentrations of mercury, a progressive increase in their hydrodynamic size is detected, with the formation of large aggregates of up to 120–170 nm at higher concentrations, as shown in Fig. 8A, while no changes in the hydrodynamic size are detected in the presence of another divalent metal (Cd^{2+}).

Although mercury and its derivatives are highly toxic and their use is completely prohibited, they are still distributed in ambient air, water, soil, and even in some foods and cosmetics. So, this type of simple inexpensive and effective mercury sensor can result in significant advantages over other traditional techniques (atomic absorption spectroscopy, inductively coupled plasma mass spectrometry and atomic fluorescence spectrometry). As shown in Fig. 8B and C, the systems developed can be highly effective at detecting mercury in different media, both in the liquid phase, by means of fluorescence emission measurements, and in the solid state, where the CuNCs also act rapidly as optical switch-off sensors for mercury detection. So, our results indicate that these new hybrid CuNCs could serve as effective fluorescent sensing probes for the facile, rapid and low-cost detection of Hg^{2+} ions with high selectivity; this type of approach has previously been reported for these kinds of hybrid systems by other authors with respect to analyzing food and cosmetics samples without any complex pretreatments,[55] water analysis[56] and biomedical applications, like the detection of Hg^{2+} in human urine and serum.[57]

Finally, for testing the practical applicability of the new hybrid CuNCs, mercury detection experiments were carried out in human urine samples without any previous purification. The results indicate the linear response of the fluorescence quenching efficiency of the polymeric CuNCs in the presence of increasing concentrations of mercury in urine, over the range from 10–100 μM, as displayed in Fig. 9B. The results demonstrate the fast and efficient response of the hybrid CuNCs in the presence of mercury in this biological medium, exhibiting a very similar response to what was obtained using these same hybrid compositions in aqueous solutions.

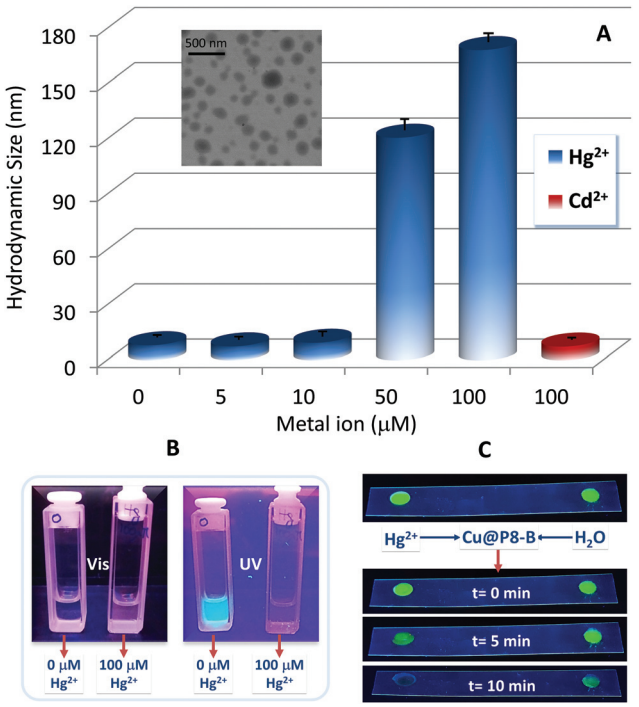

Fig. 8 (A) The hydrodynamic size data from the Cu@P6-B nanohybrids obtained *via* DLS measurements in basic (pH 12) dilute solutions (1 mg mL^{-1}) at 20 °C in the presence of increasing concentrations of Hg^{2+} (between 5 μM and 100 μM: blue bars) and in the presence of Cd^{2+} at 100 μM (red bar). Inset: An STEM image of the hybrid CuNC aggregates in the presence of 100 μM Hg^{2+}. (B) Photographs of dilute liquid solutions of Cu@P6-B obtained in the absence and presence of 100 μM Hg^{2+} under both visible and UV light. (C) Time lapsed photographs of solid deposited Cu@P6-B hybrids in the absence and presence of 100 μM Hg^{2+} under UV light.

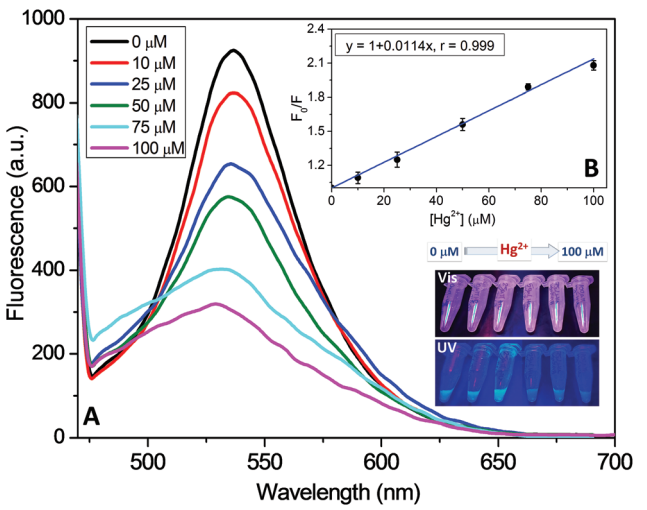

Fig. 9 (A) The evolution of the fluorescence emission spectra of Cu@P8-B nanohybrids in human urine in the presence of increasing concentrations of Hg^{2+} (between 10 μM and 100 μM) (λ_{exc} = 440 nm). (B) A Stern–Volmer representation of the Cu@P8-B hybrids in human urine quenched by Hg^{2+} (the solid blue line corresponds to the linear fit of the obtained data in the 0–100 μM range). Inset: Photographs of the Cu@P8-B nanohybrids in human urine in the presence of increasing concentrations of Hg^{2+} (between 0 μM and 100 μM) under both visible and UV light.

4. Conclusions

In this work, for the first time, fluorescent copper nanoclusters were synthesized and functionalized using thermoresponsive polymers decorated with thiol groups that acted as ligands and templates. The new bright yellow/green, water-stable and smart copper-polymer nanohybrids with pH- and thermo-responsive features were synthesized through a one-pot approach *via* a facile, green, fast and efficient synthetic procedure.

The controlled polymerization of the copolymers *via* an ATRP process allowed for the control of the thiol functionalization ratio and the molecular size of the new polymeric materials, so they could provide stable coverage of the CuNCs and maintain smaller nanometric sizes than those obtained for protein-free macroscopic aggregates; comparable luminescence properties were also preserved in aqueous solution. The simple and low cost synthetic methodology proposed here differs from other conventional methods (*e.g.*, pH-, temperature- or solvent-induced aggregation, or even sonication) used for the fabrication of optical water-soluble nanostructures with AIE behavior, and it is excellent at overcoming incompatibilities relating to the solubilities of the fluorescent aggregates formed during the AIE process.

The stable bright greenish-yellow emission in water over long periods of time, high photostability under UV irradiation and strong oxidation resistance of the hybrid CuNCs suggest the great promise of these hybrids for nanomedicine, catalysis and bioimaging applications as highly fluorescent sensors, as well as in label-free chemical and biochemical detection. In fact, the polymeric CuNCs obtained were successfully applied as highly selective and sensitive fluorescent probes for the detection of Hg^{2+} in the presence of other metal ions, both in liquid and solid states. The feasibility of the application of these new hybrid CuNCs has been assayed for Hg^{2+} detection in human urine.

The new class of nanohybrid system described here demonstrates that the design of smart supramolecular ligands, which can control the immediate environment of the CuNCs, provides not only stable CuNCs in biological environments but also gives rise to new patterns in the unique properties of both components, as well as new properties that arise from synergistic interactions between the two components.

Conflicts of interest

There are no conflicts of interest to declare.

Acknowledgements

The authors are thankful for the financial support from Ministerio de Ciencia, Innovación y Universidades (MCIU), Agencia Estatal de Investigación (AEI) and Fondo Europeo de Desarrollo Regional (FEDER, UE) through the project: PGC2018-095364-B-I00 and Ministerio de Economía y Competitividad (MINECO) through the project: MAT2014-57429-R. J. Benavides acknowledges Comunidad Autónoma de Madrid (CAM) for his predoctoral fellowship (PEJD-2017-PRE/IND-4806) through the Garantía Juvenil Program. The authors would like to thank Silvia Villar Rodil for assistance with the XPS measurements. Authors also acknowledge support of the publication fee by the CSIC Open Access Publication Support Initiative through its Unit of Information Resources for Research (URICI).

References

1 R. Jin, C. Zeng, M. Zhou and Y. Chen, *Chem. Rev.*, 2016, **116**, 10346–10413.
2 S. Maity, D. Bain and A. Patra, *J. Phys. Chem. C*, 2019, **123**, 2506–2515.
3 H. Qian, M. Zhu, Z. Wu and R. Jin, *Acc. Chem. Res.*, 2012, **45**, 1470–1479.
4 P. Khandelwal and P. Poddar, *J. Mater. Chem. B*, 2017, **5**, 9055–9084.
5 N. Goswami, Q. Yao, Z. Luo, J. Li, T. Chen and J. Xie, *J. Phys. Chem. Lett.*, 2016, **7**, 962–975.
6 Y. Guo and W. Zhao, *Analyst*, 2019, **144**, 388–395.
7 Y. Tao, M. Li, J. Ren and X. Qu, *Chem. Soc. Rev.*, 2015, **44**, 8636–8663.
8 K. Zarschler, L. Rocks, N. Licciardello, L. Boselli, E. Polo, K. P. Garcia, L. De Cola, H. Stephan and K. A. Dawson, *Nanomedicine*, 2016, **12**, 1663–1701.
9 L. Yang, H. Wang, D. Li, L. Li, X. Lou and H. Liu, *Chem. Mater.*, 2018, **30**, 5507–5515.
10 X. Wang, S. Xu and W. Xu, *Nanoscale*, 2011, **3**, 4670–4675.
11 N. N. M. Adnan, S. Ahmad, R. P. Kuchel and C. Boyer, *Mater. Chem. Front.*, 2017, **1**, 80–90.
12 X. Liu and D. Astruc, *Coord. Chem. Rev.*, 2018, **359**, 112–126.
13 Z. Wang, B. Chen and A. L. Rogach, *Nanoscale Horiz.*, 2017, **2**, 135–146.
14 X. Jia, X. Yang, J. Li, D. Li and E. Wang, *Chem. Commun.*, 2014, **50**, 237–239.
15 K. T. Prakash, N. Singh and V. Venkatesh, *Chem. Commun.*, 2019, **55**, 322–325.
16 Y. Guo, F. Cao, X. Lei, L. Mang, S. Cheng and J. Song, *Nanoscale*, 2016, **8**, 4852–4863.
17 W. J. Zhang, S. G. Liu, L. Han, Y. Ling, L. L. Liao, S. Mo, H. Q. Luo and N. B. Li, *Anal. Methods*, 2018, **10**, 4251–4256.
18 R. Rajamanikandan and M. Ilanchelian, *Anal. Methods*, 2018, **10**, 3666–3674.
19 H. Li, C. Wang, P. Gai, T. Hou, L. Ge and F. Li, *RSC Adv.*, 2016, **6**, 76679–76683.
20 L. Ruiyi, W. Huiying, Z. Xiaoyan, L. Xiaoqing, S. Xiulan and L. Zaijun, *New J. Chem.*, 2016, **40**, 732–739.
21 Y. Huang, H. Feng, W. Liu, S. Zhang, C. Tang, J. Chen and Z. Qian, *J. Mater. Chem. B*, 2017, **5**, 5120–5127.

22 M. Zhao, H. Feng, J. Han, H. Ao and Z. Qian, *Anal. Chim. Acta*, 2017, **984**, 202–210.
23 X. Su and J. Liu, *ACS Appl. Mater. Interfaces*, 2017, **9**, 3902–3910.
24 J. Feng, Y. Chen, Y. Han, J. Liu, S. Ma, H. Zhang and X. Chen, *ACS Omega*, 2017, **2**, 9109–9117.
25 Y. Liu, D. Yao and H. Zhang, *ACS Appl. Mater. Interfaces*, 2018, **10**, 12071–12080.
26 M. Liras, O. Garcia, N. Guarrotxena, M. Palacios-Cuesta and I. Quijada-Garrido, *Polym. Chem.*, 2013, **4**, 5751–5759.
27 M. Liras, E. Peinado, P. Cañamero, I. Quijada-Garrido and O. García, *J. Polym. Sci., Part A: Polym. Chem.*, 2014, **52**, 3087–3095.
28 M. Liras, I. Quijada-Garrido, M. Palacios-Cuesta, S. Muñoz-Durieux and O. García, *Polym. Chem.*, 2014, **5**, 433–442.
29 M. Liras, I. Quijada-Garrido and O. García, *Polym. Chem.*, 2017, **8**, 5317–5326.
30 M. Liras, M. González-Béjar, E. Peinado, L. Francés-Soriano, J. Pérez-Prieto, I. Quijada-Garrido and O. García, *Chem. Mater.*, 2014, **26**, 4014–4022.
31 N. Garcia-Bosch, M. Liras, I. Quijada-Garrido and O. García, *RSC Adv.*, 2016, **6**, 67643–67650.
32 D. Magde, R. Wong and P. G. Seybold, *Photochem. Photobiol.*, 2002, **75**, 327–334.
33 S. Medel, J. M. García, L. Garrido, I. Quijada-Garrido and R. París, *J. Polym. Sci., Part A: Polym. Chem.*, 2011, **49**, 690–700.
34 J.-F. Lutz and A. Hoth, *Macromolecules*, 2006, **39**, 893–896.
35 C. Wang, H. Cheng, Y. Huang, Z. Xu, H. Lin and C. Zhang, *Analyst*, 2015, **140**, 5634–5639.
36 C. Weber, R. Hoogenboom and U. S. Schubert, *Prog. Polym. Sci.*, 2012, **37**, 686–714.
37 A. K. Teotia, H. Sami and A. Kumar, in *Switchable and Responsive Surfaces and Materials for Biomedical Applications*, ed. Z. Zhang, Woodhead Publishing, Oxford, 2015, pp. 3–43, DOI: 10.1016/B978-0-85709-713-2.00001-8.
38 X. An, H. Liu, J. Qu, S. J. A. Moniz and J. Tang, *New J. Chem.*, 2015, **39**, 314–320.
39 J. Xu and B. Han, *Nano*, 2016, **11**, 1650108.
40 K. E. Knowles, K. H. Hartstein, T. B. Kilburn, A. Marchioro, H. D. Nelson, P. J. Whitham and D. R. Gamelin, *Chem. Rev.*, 2016, **116**, 10820–10851.
41 A. Heuer-Jungemann, N. Feliu, I. Bakaimi, M. Hamaly, A. Alkilany, I. Chakraborty, A. Masood, M. F. Casula, A. Kostopoulou, E. Oh, K. Susumu, M. H. Stewart, I. L. Medintz, E. Stratakis, W. J. Parak and A. G. Kanaras, *Chem. Rev.*, 2019, **119**, 4819–4880.
42 T. Long, Y. Guo, M. Lin, M. Yuan, Z. Liu and C. Huang, *Nanoscale*, 2016, **8**, 9764–9770.
43 Z. Miao, W. Hou, M. Liu, Y. Zhang and S. Yao, *New J. Chem.*, 2018, **42**, 1446–1456.
44 U. Sivasankaran, J. Radecki, H. Radecka and K. Girish Kumar, *Luminescence*, 2019, **34**, 243–248.
45 Y.-S. Borghei, M. Hosseini, M. Khoobi and M. R. Ganjali, *J. Fluoresc.*, 2017, **27**, 529–536.
46 Y. Li, L. Feng, W. Yan, I. Hussain, L. Su and B. Tan, *Nanoscale*, 2019, **11**, 1286–1294.
47 X. Bu, Y. Fu, H. Jin and R. Gui, *New J. Chem.*, 2018, **42**, 17323–17330.
48 D. Li, G. Wang, Y. Peng, Z. Chen, X. Gao, L. Cheng and X. Mei, *Nanoscale Adv.*, 2019, **1**, 1086–1095.
49 H. Huang, H. Li, A.-J. Wang, S.-X. Zhong, K.-M. Fang and J.-J. Feng, *Analyst*, 2014, **139**, 6536–6541.
50 M. Hembury, N. Beztsinna, H. Asadi, J. B. van den Dikkenberg, J. D. Meeldijk, W. E. Hennink and T. Vermonden, *Biomacromolecules*, 2018, **19**, 2841–2848.
51 P. Yu, X. Wen, Y.-R. Toh and J. Tang, *J. Phys. Chem. C*, 2012, **116**, 6567–6571.
52 S. Chandra, G. Beaune, N. Shirahata and F. M. Winnik, *J. Mater. Chem. B*, 2017, **5**, 1363–1370.
53 A. Ferrández-Montero, I. Quijada-Garrido, M. Liras and O. García, *Eur. Polym. J.*, 2016, **84**, 565–576.
54 K. Morishita, J. L. MacLean, B. Liu, H. Jiang and J. Liu, *Nanoscale*, 2013, **5**, 2840–2849.
55 J. Liu, Y. Chen, W. Wang, J. Feng, S. Peng, S. Ma, H. Chen and X. Chen, *RSC Adv.*, 2016, **6**, 89916–89924.
56 X. Hu, W. Wang and Y. Huang, *Talanta*, 2016, **154**, 409–415.
57 X. Yang, Y. Feng, S. Zhu, Y. Luo, Y. Zhuo and Y. Dou, *Anal. Chim. Acta*, 2014, **847**, 49–54.